Silk Macromolecules with Amino Acid–Poly(Ethylene Glycol) Grafts for Controlling Layer-by-Layer Encapsulation and Aggregation of Recombinant Bacterial Cells

Irina Drachuk,[†] Rossella Calabrese,[‡] Svetlana Harbaugh,[§] Nancy Kelley-Loughnane,[§] David L. Kaplan,[‡] Morley Stone,[§] and Vladimir V. Tsukruk*,[†]

[†]School of Materials Science and Engineering, Georgia Institute of Technology, Atlanta, Georgia 30332, United States, [‡]Department of Biomedical Engineering, Tufts University, Medford, Massachusetts 02155, United States, and [§]Air Force Research Laboratory, Directorate of Human Effectiveness, Wright-Patterson AFB, Dayton, Ohio 45433, United States

ABSTRACT This study introduces double-brush designs of functionalized silk polyelectrolytes based upon regenerated silk fibroin (SF), which is modified with poly-L-lysine (SF-PLL), poly-L-glutamic acid (SF-PGA), and poly(ethylene glycol) (PEG) side chains with different grafting architecture and variable amino acid-PEG graft composition for cell encapsulation. The molecular weight of poly amino acids (length of side chains), molecular weight and degree of PEG grafting (*D*) were varied in order to assess the formation of cytocompatible and robust layer-by-layer (LbL) shells on two types of bacterial cells (Gram-negative and Gram-positive bacteria). We observed that shells assembled with charged polycationic amino acids adversely effected the properties of microbial cells while promoting the formation of large cell aggregates. In contrast, hydrogen-bonded shells with high PEG grafting density were the most cytocompatible, while promoting formation of stable colloidal suspensions of individual cell encapsulates. The stability to degradation of silk shells (under standard cell incubation procedure) was related to the intrinsic properties of thermodynamic bonding forces, with shells based on electrostatic interactions having stronger resistance to deterioration compared to pure hydrogen-bonded silk shells. By optimizing the charge density of silk polyelectrolytes brushes, as well as the length and the degree of PEG side grafts, robust and cytocompatible cell coatings were engineered that can control aggregation of cells for biosensor devices and other potential biomedical applications.

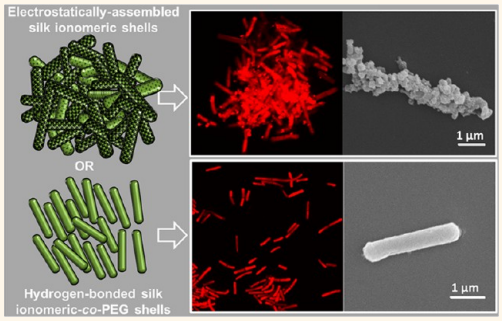

KEYWORDS: brush silk polyelectrolytes · layer-by-layer (LbL) assembly · bacterial cells · hydrogen bonded shells

The innate organization of microbial cells in the form of biofilms, cell clusters or aggregates plays an important factor not only in cells survivability, but also in regulation of gene expression.[1−4] One of the fundamental processes in microbiology is cell–cell communication, termed quorum sensing (QS), that allows bacteria to monitor the environment and to alter behavior on a population-wide scale in response to changes in the cell number and/or species present in the community.[2,5] Recently, the concept of efficiency sensing was proposed, in which cells sense a combination of cell density, mass-transfer properties and spatial cell distribution to respond accordingly when concentration of extracellular effectors is efficient.[6] Active formation of bacterial cells into aggregates (biofilms) supported by extracellular polymer matrix can significantly protect them from different antibacterial agents and even human defense system.[7,8] On the other hand, confinement-induced individual cells can produce the same level of QS effectors (under plausible natural conditions) in order to activate the virulence factors needed for survival.[9,10]

Modification of cell surfaces with nanothin shells composed of functionalized macromolecules and nanoparticles of natural and synthetic origins can provide

* Address correspondence to vladimir@mse.gatech.edu.

Received for review August 30, 2014 and accepted January 14, 2015.

Published online January 14, 2015
10.1021/nn504890z

© 2015 American Chemical Society

means for gaining novel structures and multifunctional properties that are otherwise unattainable in the native, nonencapsulated state.[11−17] For example, nanoshells with adjustable stiffness, increased mechanical robustness, switchable adhesion or controlled enzyme-resistant activity provide opportunities for actively manipulating biophysical properties of cells at the cell−shell interface.[18−25]

Recently, we have demonstrated the formation of protein coatings assembled from pure regenerated silk fibroin (SF), which allows the modification of cell surfaces with cytocompatible shells that undergo relatively rapid intracellular degradation, thereby only providing short-term protection.[26] As an alternative, chemically modified SF proteins with charged amino acid side chains can enrich silk-based coatings with new properties, such as enhanced mechanical stiffness and tailored protein absorption.[27,28] Variations in grafting density (*D*), as well as in the length and conformation of charged amino acids attached to the backbone of the silk protein might influence the chemical interactions involved in the layer-by-layer (LbL) assembly of macromolecules, and, as the result, affect the properties of the shells. Moreover, the adsorption of the same macromolecules at different cell surfaces would potentially mediate protein immobilization and may result in directed assembly of silk macromolecules at nano- and macroscale levels as was demonstrated with synthetic polymers during bacteria-instructed synthesis.[29]

The robustness of LbL films assembled *via* attractive interactions between oppositely charged polyelectrolytes is significantly affected by the charge density,[30] the degree of ionization,[31] molecular weight,[32] secondary intermolecular interactions and the structural architecture[33] of the polymers under specific assembly conditions.[34−37] Conventional polyelectrolyte LbL shells, which form ultrathin cell coatings interfere with cell viability, a major factor in assessing shells efficacy for biofunctional protection of encapsulated cells.[38−40] The severity of cytotoxicity depends on molecular weight, charge density and concentration of polycationic component.[41] One of the current strategies for reducing the cytotoxicity of polycations during cell surface modification involves decreasing the charge density by grafting poly(ethylene glycol) (PEG) chains along the polycation chain.[42−44] With sufficient length and degree of grafting, films assembled with PEG copolymers could be rendered cytocompatible while simultaneously facilitating robust LbL film assembly based on electrostatic interactions with its negatively charged counter-polymer.[45−47]

Here, we report how assembly of LbL shells composed from complex silk brushes with variable architecture and grafting density of mixed amino acid/polyethylene glycol side grafts can render distinct morphological and spatial organization of the cells-in-shells structures. Four different shell compositions have been studied that resulted in distinct appearance of encapsulated cells, as well as affected the viability and activity of recombinant cells. We also assessed how the bacterial surface properties can influence the adsorption of charged protein brushes during LbL assembly and impact the clustering of the cells. We demonstrated that silk shells prepared from graft PEG copolymers of optimal grafting density and architecture promoted desirable spatial organization of the individual cells while protecting their capacity to selectively respond to specific chemical analytes.

RESULTS AND DISCUSSION

Modification of Silk Fibroin with Polyamino Acids. Regenerated silk fibroin protein was modified with poly-L-lysine (PLL) and poly-L-glutamic acid (PLA) with different molecular weight and grafting densities in order to obtain amino acids functionalized silk polyelectrolytes (ionomers) with high and low charge densities (Table 1a−d).[48] A high degree of derivation of silk ionomers, namely SF(Y,S)-PLL and SF(Y,S)-PGA, was achieved by grafting highly dispersed in M_w ($M_w \leq$ 15 kDa) long chains of polyamino acids to tyrosine (Y) and serine (S) residues of carboxylate-modified SF (SF(Y,S)-COOH), which accounted for ∼18 mol % modification of the available amino acids in SF (Table 1a,b). The increase in charge density allowed efficient charge−charge interactions during electrostatic LbL assembling of modified silk proteins. Low charge density silk ionomers were obtained by grafting PLL or PGA chains of low molecular weight (M_w = 3 kDa) to serine residues only of SF(S)-COOH intermediate (Table 1c,d). The degree of derivation for SF(S)-PLL and SF(S)-PGA was calculated to be 0.1 and 0.9 mol % in terms of moles of amino acids in SF macromolecule modified with PLL or PGA, respectively (Table 1c,d).[49,50]

To improve the biological compatibility of the functionalized silk backbones during LbL assembly at cell surfaces, double brush-like PEG-grafted silk copolymers were prepared with different grafting structures (see Methods and Table 1 for general representation of brush silk backbones synthesized here). Double brush graft (*g*) SF(Y,S)-PLL-*g*[*D*]-PEG copolymer was synthesized by conjugation PEG (M_w = 5 kDa) to high charge density SF(Y,S)-PLL silk ionomer with variable grafting degrees, designated as *D* (Table 1e). The grafting degree refers to the molar percentage of PEG groups grafted to each PLL side chain (Figure S1, Supporting Information, ^{1}H NMR). ^{1}H NMR analysis confirmed successful modification of SF(Y,S)-PLL silk ionomer with 4 mol % and 9 mol % degree of grafting, further referred as SF(Y,S)-PLL-*g*[4]-PEG and SF(Y,S)-PLL-*g*[9]-PEG double PEG brushes (Figure S1−S4). In terms of the number of amino acids actually modified with PLL and PEG side chains, approximately ∼900 amino acids (out of the total 5300 residues)[49] had PLL attached to the backbone of the SF molecule with 5 (4 mol %) or 11 (9 mol %) PEG chains conjugated to each PLL side chain.

TABLE 1. Summary Table of Silk Brushes Grafted with Different Amino Acids and PEG Chains Used for LbL Encapsulation of Bacterial Cells

	Abbreviation and Schematic Presentation of Silk Copolymers	Degree of SF derivation	Molecular weight of side chains	Chemical structure
High charge density silk ionomers	a) SF (Y,S)-PLL 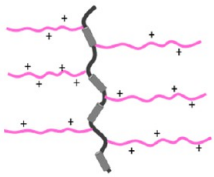	~ 18 mol% (theoretical calculations)	15 kDa	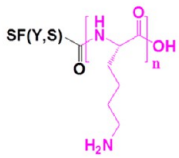
	b) SF(Y,S)- PGA 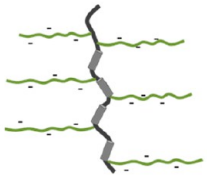	~ 18 mol% (theoretical calculations)	15 kDa	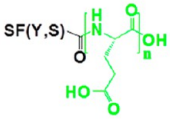
Low charge density silk ionomers	c) SF(S)-PLL 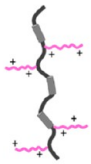	0.1 mol% (^{1}HNMR)	3 kDa	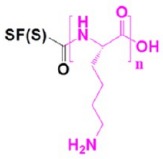
	d) SF(S)-PGA 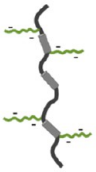	0.9 mol% (^{1}HNMR)	3 kDa	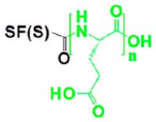
Double-brush PEG-graft silk copolymer	e) SF(Y,S)-PLL-*g*[*D*]-PEG 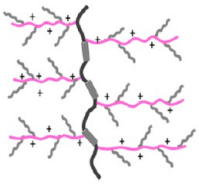	4 mol% and 9 mol% (^{1}HNMR)	15 kDa (for PLL) 5 kDa (for PEG)	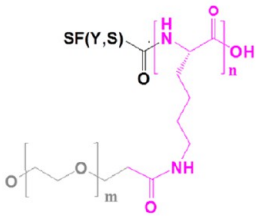
Brush PEG-block silk copolymer	f) SF(S)-PLL-*b*-PEG 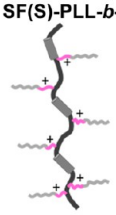	0.5 mol% (^{1}HNMR)	2.6 kDa	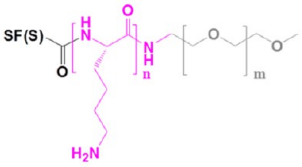

Alternatively, the brush-like block SF(S)-PLL-*b*-PEG copolymer was obtained by conjugating PLL_{10}-PEG_{22} (M_w = 2.6 kDa) block copolymer to the SF(S)-COOH carboxylate-modified silk (Table 1f). Calculated by the amino acid composition analysis, grafting degree for the SF(S)-PLL-*b*-PEG block copolymer was 0.5 mol %, which accounts for ~27 amino acid residues being conjugated to form the SF(S)-PLL-*b*-PEG block copolymer.

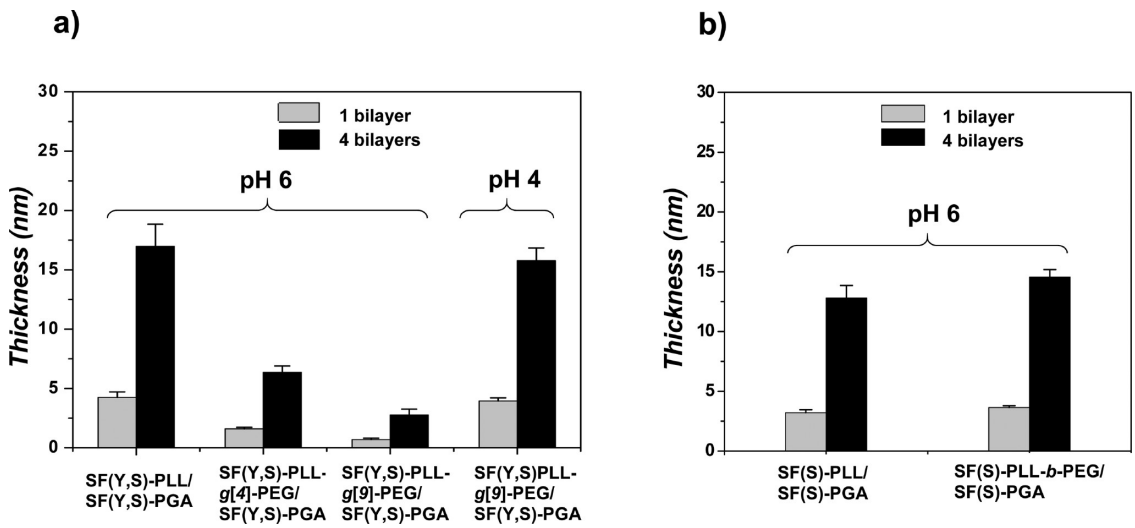

Figure 1. Thickness of 1 and 4 bilayered films in the dry state (measured by ellipsometry method) as a function of charge density, degree of PEGylation, and assembly conditions for *high charge* density (a) and *low charge* density (b) silk copolymers. Braces represent pH conditions, at which the films have been prepared during dip-assisted LbL deposition. Experimental values are represented as means ± SD, *n* = 3.

LbL Assembly of SF Polyelectrolyte Films. Ellipsometry measurements of four bilayered LbL films with variable charge density, length and architecture of PEG grafts were performed in order to assess LbL deposition of various functionalized silk backbones at different conditions. Figure 1 provides a comparison of the film thickness for two systems of silk ionomers adsorbed on planar substrates during dip-assisted LbL deposition. As expected, high charge density SF polyelectrolytes demonstrated strong adsorption at pH 6 with 4.2 ± 0.5 nm thickness per single bilayer, which was comparable to strongly bound synthetic polymers.[36] Brush silk graft copolymers with PEG chains consistently hindered adsorption of monolayers during LbL-assembly with silk anionic polyelectrolyte, specifically when the deposition was performed at pH 6. With increasing the grafting degree of PEG side chains the potential for electrostatic interactions necessary to drive film assembly was hindered by steric effects of densely packed polyether side chains. Consequently, the graft copolymer with grafting ratio of 9 mol % (SF(Y,S)-PL-*g*[9]-PEG) demonstrated the lowest film thickness with only 0.7 ± 0.1 nm bilayer thickness at pH 6, which is below expected thickness for two backbones. In order to improve the assembly of LbL films with highly PEGylated silk copolymers brushes, the driving forces of intermolecular interactions were switched from electrostatic to hydrogen-bonding by lowering the pH of LbL assembly to 4 (the reported pK_a of poly-L-glutamic acid is 4.07). As a result of this modification, the film thickness significantly increased to 4.0 ± 0.3 nm per bilayer (Figure 1a). In comparison to other hydrogen-bonded systems based on synthetic polymers of comparable weight, films with silk double brush copolymers demonstrated comparable thickness of bilayers mainly due to the bulky conformational composition of the silk macromolecules and distinct trend of the silk fibroin to self-assemble.[51−53]

The assembly of low charge silk polyelectrolytes maintained modest adsorption at pH 6 (when both species have effective counter-charges necessary to drive LbL assembly) with bilayer thickness of 3.2 ± 0.3 nm (Figure 1b). With stoichiometric uneven pairing between low charge density silk ionomers (0.1 mol % for SF(S)-PLL and 0.9 mol % for SF(S)-PGA), the driving forces for intermolecular interactions seem to be more complex generating stable multilayer films with interpenetrated internal structure.[36] Interestingly, films assembled from brush-like PEG block copolymers demonstrated statistically similar values for the film thickness (3.6 ± 0.2 nm) with the low charge density silk polyelectrolytes (paired *t* test, $p < 0.05$). The higher degree of derivation (0.5 mol %) of the silk block copolymer SF(S)-PLL-*b*-PEG could account for the stronger absorption of silk macromolecules *via* mostly hydrogen bonding and hydrophobic interactions that are similar to low charge density silk ionomers internal film structure.

Formation of LbL Shells on Bacterial Cells. Deposition of silk polyelectrolyte LbL shells with different chemistry and their effect on cell behavior was assessed on two types of recombinant bacterial cells engineered with synthetic riboswitch constructs: Gram-negative (*Escherichia coli*) and Gram-positive (*Bacillus subtilis*) cells.[74] Even though both types of bacteria are rod-shaped, the architecture of their cell envelopes differs significantly in terms of cell membrane/cell wall design and chemical composition.[54,55] Because of the striking variance in chemical nature of the cell surfaces, the adsorption of the same macromolecules may provoke distinct changes in the cell coatings and overall colloidal behavior of cells-in-shells assemblies. This phenomenon will be discussed in detail further.

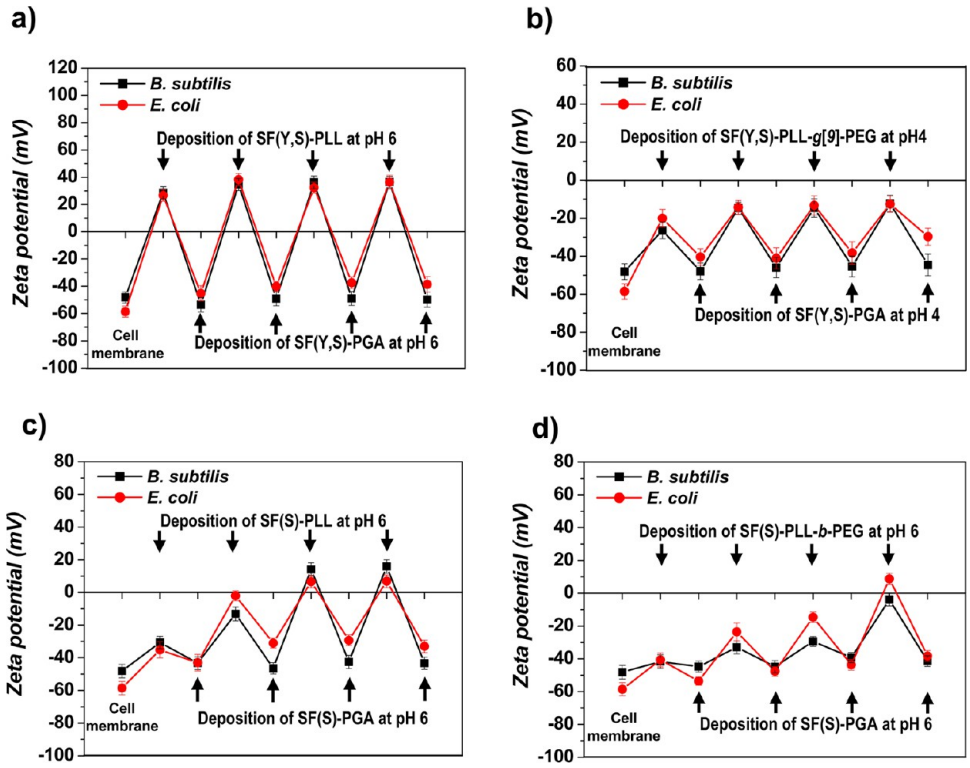

Figure 2. Zeta-potential (from aqueous solutions) after adsorption of a single layer during LbL-assembly of silk polyelectrolytes on two types of bacterial cells (*E. coli* and *B. subtilis*) as a result of intermolecular interactions: strong electrostatic interactions with *high charge* density SF(Y,S)-PLL and SF(Y,S)-PGA silk polyelectrolytes (a), pure hydrogen-bonded interactions with highly PEGylated double brush SF(Y,S)-PLL-*g*[9]-PEG silk graft copolymer (b), weak electrostatic interactions with *low charge* density SF(S)-PLL and SF(S)-PGA silk polyelectrolytes (c) and combination of interactions based on weak electrostatic, hydrogen-bonded, van der Waals and hydrophobic bondings with brush-like SF(S)-PLL-*b*-PEG silk block copolymer (d). Experimental values are represented as means ± SD, *n* = 6.

Assembly of silk polyelectrolytes on cells was monitored by measuring Zeta-potential of encapsulated cells after adsorption of a single layer during alternating LbL steps (see Methods section for details). Figure 2 represents changes in the surface charges acquired as a result of noncovalent interactions between silk proteins of different compositions. An example of surface charge compensation for highly charged silk polyelectrolytes at pH 6 is represented in Figure 2a. With highly PEGylated double brush silk polyelectrolyte backbones (SF(Y,S)-PLL-*g*[9]-PEG), the assembly of silk shells was carried at pH 4 to promote hydrogen-bond interactions with a protonated counterpart specie, SF(Y,S)-PGA (Figure 2b). Since the assembly relied on hydrogen bonding between ether groups of PEG chains and carboxylate groups of SF(Y,S)-PGA chains, the charge reversal was hindered suggesting that significant numbers of unprotonated chains were responsible for the negative values of Zeta-potential and overall good colloidal stability of cells-in-shells structures.

It is worth noting that among the intermolecular forces (predominated interactions) between functionalized silk proteins, the existence of intramolecular forces should also be accounted. The intermolecular interactions might compete with the self-assembly of protein macromolecules since the transition of the silk fibroin from random coils into secondary structures: silk II (β-sheets) or silk III (α-helices) can be easily induced by many factors during LbL assembly (reduced pH, increased ionic strength and molarity of solute buffers, elevated temperatures, sheer stresses).[56−58] Nonspecific interactions (van der Waals, hydrophobic and hydrogen bond forces) induced by the presence of such effectors might promote formation of complex transitions that can either complement or compete with intermolecular forces during the LbL assembly of macromolecules. In the former case, the formation of stable and smooth films is more promoted, while in the latter case, when protein self-assembly is dominant, less stable and rather rough LbL films can be produced as was demonstrated elsewhere.[59,60]

Assembly of silk polyelectrolytes with low charge density on bacteria surfaces demonstrated minimal effect of side chains mainly due to the low degree of derivation (0.1 mol % for SF(S)-PLL and 0.9 mol % for SF(S)-PGA) and short side chains (n = 20) of polyamino acids. The surface charges associated with deposition of polycationic silk fluctuated in negative range values for the first two alternating cycles, and then gradually moved to positive values during the last two deposition cycles (Figure 2c). On the basis of the thickness build-up and Zeta-potential trend, the adsorption of

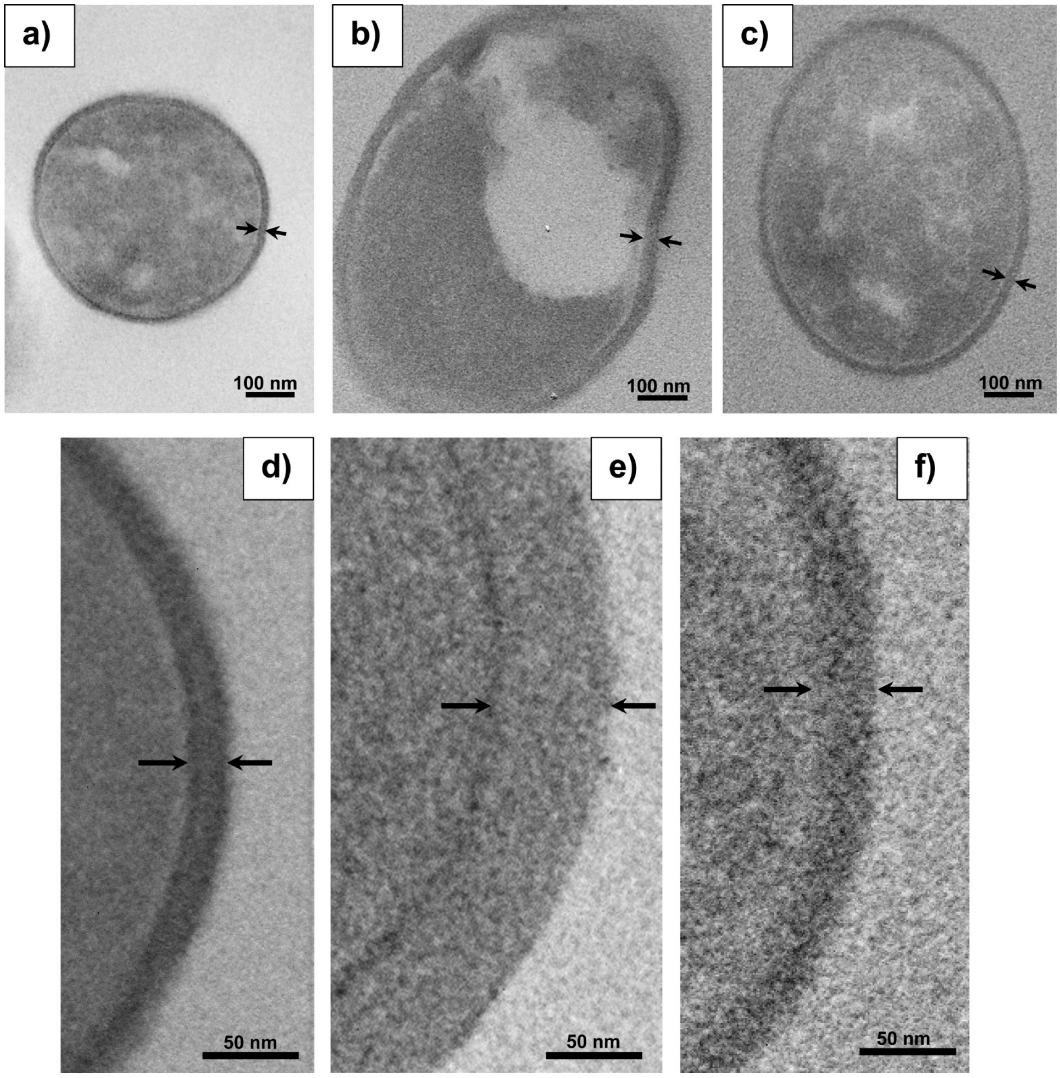

Figure 3. Cross-sectional TEM images of *B. subtilis* cells (control, (a, d)) encapsulated in high charge density SF(Y,S)-PLL/SF(Y,S)-PGA silk ionomer shells (b, e) and highly PEGylated double brush graft copolymer (SF(Y,S)-PLL-*g*[9]-PEG/SF(Y,S)-PGA) shells (c, f).

silk polyelectrolytes with low charge grafting density seems to rely on other nonspecific (*i.e.*, nonionic) interactions that permit the formation of stable silk LbL shells. During LbL assembly with brush-like PEGylated silk block copolymer, the adsorption of silk macromolecules was supported by nonspecific interactions (hydrogen-bonding, van der Waals and hydrophobic forces), as can be observed by predominant fluctuation of Zeta-potential within negative range (Figure 2d).

In order to prove the adsorption of silk brush copolymers at the cell surfaces and estimate the thickness of absorbed LbL shells directly on the cells, some transmission electron microscopy (TEM) images of bare and encapsulated bacteria were collected (Figure 3). It is worth to note that in conventional preparations for TEM, the extraction and shrinkage of essential cell envelope constituents as well as externally assembled polymer shells can occur during fixing, dehydration and embedding of cells.[61,62]

Cross-sectional images of *B. subtilis* cells revealed the presence of fine conformal coatings surrounding the bacteria. Even nonencapsulated cells had distinct appearance of the "non-specific" coating, which is associated with the staining of bacterial polysaccharides with heavy metal salts and is referred as native cell envelope.[63] The observed thickness of "electron-dense" cell cortex was 15.5 $\pm$ 2.1 nm (Figure 3a). After encapsulation in silk ionomer shells with high charge density, the thickness of the overall stained coating increased twice, to 31.7 $\pm$ 3.6 nm (Figure 3b). Cells encapsulated in hydrogen-bonded shells with highly PEGylated double-brush SF(Y,S)-PLL-*g*[9]-PEG graft silk copolymer demonstrated increase in the coating thickness by 33% to 20.6 $\pm$ 2 nm (Figure 3c). The shell thicknesses determined by TEM imaging directly on cells were similar to those measured for the planar films evaluated by the ellipsometry. Hydrogen-bonded LbL films were thicker than corresponding shells. However, electrostatically assembled LbL films

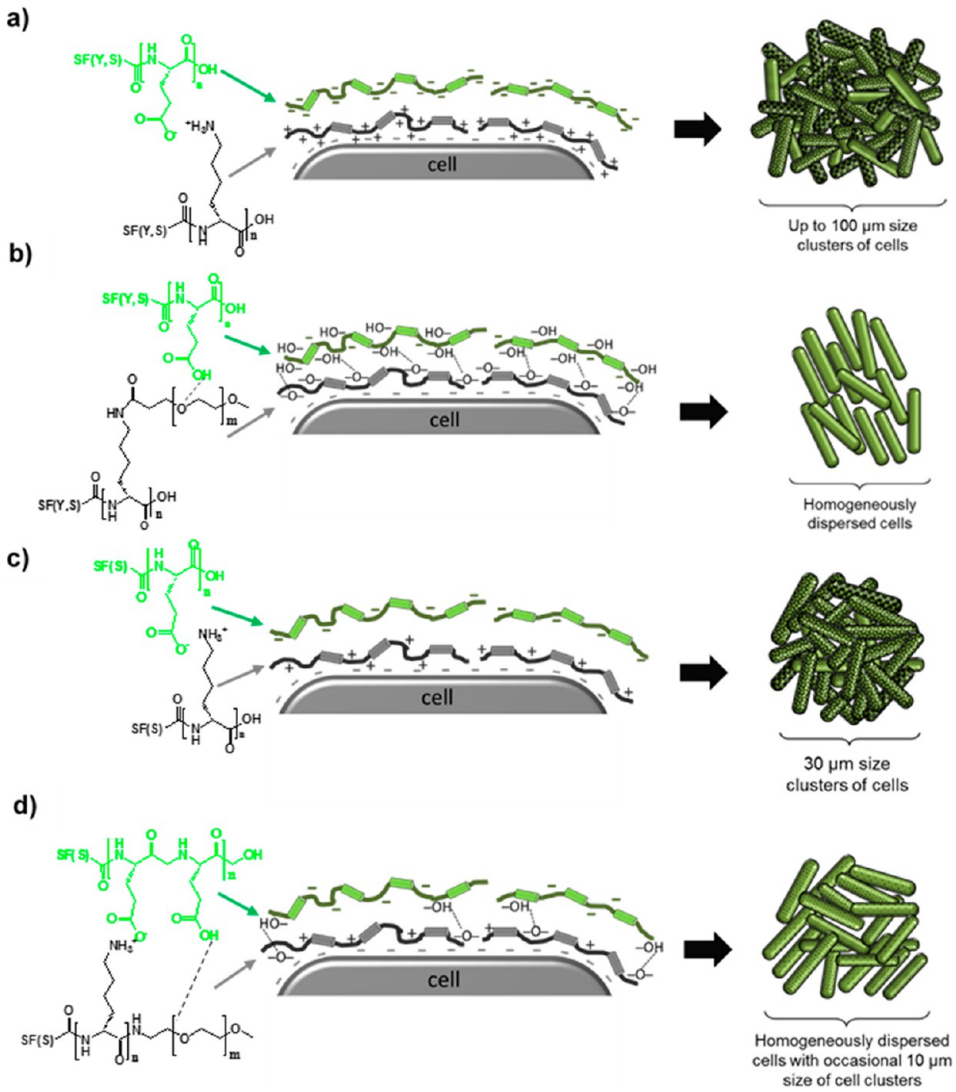

Figure 4. Scheme representing cell clustering during LbL encapsulation with different silk copolymers described in Table 1. Effect of intermolecular interactions on aggregation behavior of cells as was observed with confocal and SEM imaging: strong electrostatic bonding (a), pure hydrogen bonding (b), weak electrostatic bonding (c), complex weak electrostatic, hydrogen bonding and van der Waals interactions (d).

were similar in thickness with corresponding shells assembled on cells.

Behavior of Bacterial Cells Encapsulated in Silk Polyelectrolyte Shells. Variance in intermolecular interactions as the result of variation in grafting density and architecture of polyamino acids/PEG side chains in silk macromolecules had strong consequences on the distinct morphological appearance of coated cells, as well as on the cells aggregation behavior. Figure 4 represents a schematic visualization of different silk copolymers used for LbL cell encapsulation and highlights the effect of charge density in silk polyelectrolytes, and hence intermolecular forces involved in the formation of shells on spatial organization of cells. Adsorption of high charge density silk polyelectrolytes induced strong aggregation of cells in the form of random 40−100 μm size clusters (Figure 4a). In constrast, hydrogen bonding forces predominate between highly PEGylated double-brush SF(Y,S)-PLL-*g*[9]-PEG graft silk copolymer and protonated SF(S,Y)-PGA silk ionomer promoted single-cell encapsulates regardless of the cell type, and lead to the formation of smooth coatings and well-dispersed cells suspensions (Figure 4b). Low charge density brush-like silk polyelectrolytes assembled *via* weak electrostatic interactions resulted in reduced aggregation of cells (up to 30 μm) (Figure 4c), while brush-like shells containing SF(S)-PLL-*b*-PEG block copolymer promoted more smooth coverage of cells with occasional aggregation of cells in midsized clusters (up to 10 μm) (Figure 4d).

Figures 5 and 6 show confocal optical microscopy, SEM, and AFM images illustrating distinct changes in surface morphology after encapsulation in high charge density silk polyelectrolyte (SF(Y,S)-PLL/SF(Y,S)-PGA)$_4$ shells (Figures 5a, 6a) and hydrogen-bonded (SF(Y,S)-PLL-*g*[9]-PEG/SF(Y,S)-PGA)$_4$ shells from PEG

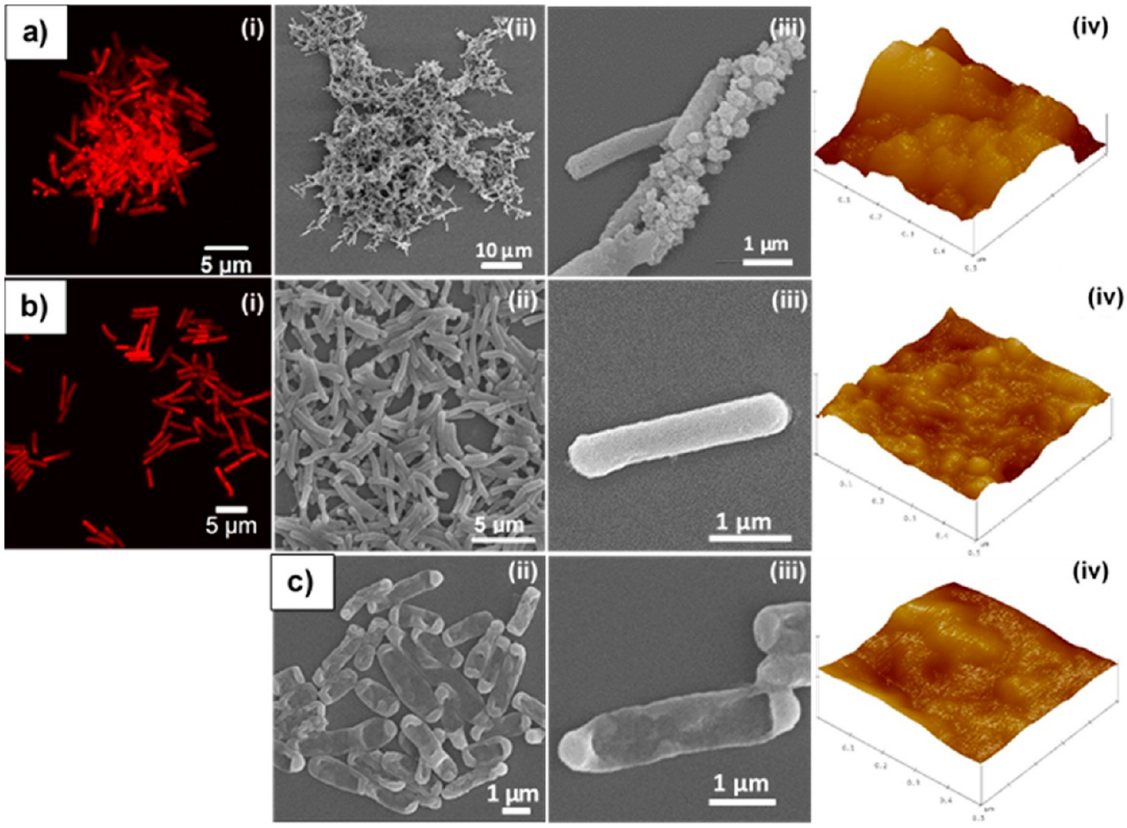

Figure 5. ***B. subtilis*** **cells encapsulated in 4 bilayers of** ***high charge*** **density SF(Y,S)-PLL/SF(Y,S)-PGA silk ionomer shells (a) and highly PEGylated double brush graft copolymer (SF(Y,S)-PLL-*g*[9]-PEG/SF(Y,S)-PGA) shells (b) in comparison to control nonencapsulated cells (c) imaged with confocal (i), SEM (ii, iii) and AFM (iv) microscopy (from 1 μm^2 surface area). Z-range in (iv) is 100 nm. Here and below: AFM scanning of 1 $\times$ 1 μm^2 area were conducted on average for 4−5 different cells. SEM scanning was done of large area of cells (at least 100 $\times$ 100 μm^2, up to 200 cells in total) and then zoomed in to show clusters of cells or individual cells presented in figures.**

double-brush silk graft copolymers (Figures 5b, 6b). As shown on the micrographs, the aggregation of cells during LbL deposition was characteristic for high charge density silk polyelectrolyte shells assembled *via* electrostatic interactions. The size of cell agglomerates was cell-specific and ranged between 20 to 40 μm for *B. subtilis* cells (Figure 5a), and between 50 to 100 μm for *E. coli* cells (Figure 6a). This emphasizes the significance of the cell surface structure and chemical composition of the cell envelope on the adsorption of protein macromolecules and ultimately, aggregation behavior of cells. As apparent from Figures 5 and 6, *E. coli* cells readily promoted formation of larger aggregates, while *B. subtilis* generated only modest cell clusters. The distinct feature of Gram-negative bacteria cells (*e.g.*, *E. coli*) is the presence of a lipopolysaccharide outer membrane.[64] This large complex molecule is anchored to the underlying peptidoglycan cell wall and has a polysaccharide chain extending outward up to 10 nm from the cell surface.[65] The abundance of these long chains and their aggregation make the cell surface appear rough. In contrast, Gram-positive bacteria (*e.g.*, *B. subtilis*) have a thick peptidoglycan cell wall consisting of sugars and amino acids that form a mesh-like layer outside of the cell membrane.[66] This suggested that binding of silk macromolecules at structurally more flat cell surfaces generated smoother coatings and hence, involved in less cell aggregation, while architecturally rough cell surfaces were contributing to the formation of coarse coatings that promoted cells clustering during adsorption of the same silk copolymers.

In addition to cell aggregation, increased surface microroughness was observed for silk LbL shells assembled *via* strong electrostatic interactions when adsorption of high-charge density proteins can favor globular conformations of polyelectrolyte proteins.[67] During deposition of functionalized silk polyelectrolyte macromolecules (specifically with high degree of derivation and long amino acid side chains) on cell surfaces, conformational changes of protein brushes resulted in significant number of unbound amino acid residues readily available for the interactions with incoming proteins of opposite charge.[67] As a consequence, intermixing of long amino acid chains with charged groups might further induce protein aggregation and formation of nanoparticles (from 50 to 300 nm in size) from highly segregated diphilic macromolecules that abundantly decorated the surface of the cells after encapsulation (Figures 5a, 6a).

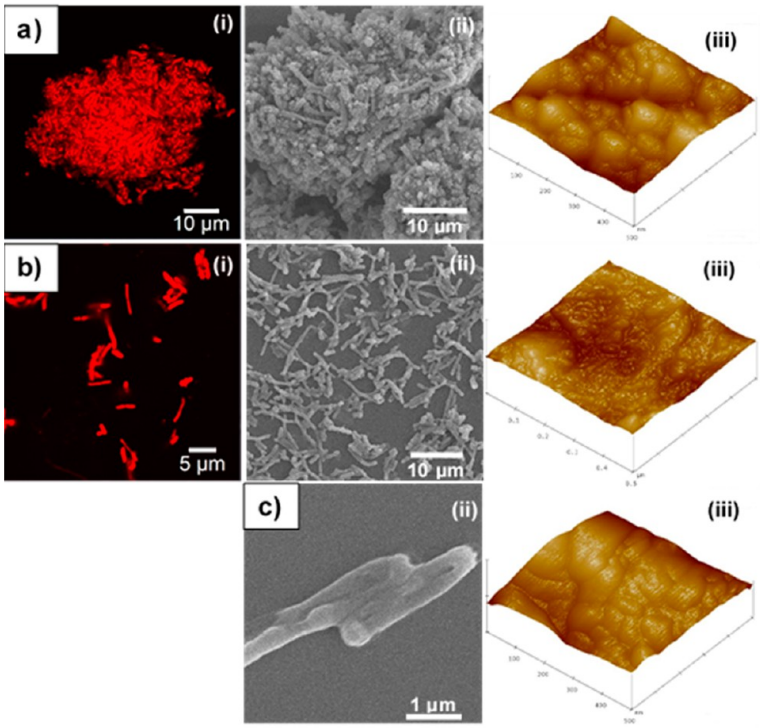

Figure 6. ***E. coli*** **cells encapsulated in 4 bilayers of** ***high charge*** **density SF(Y,S)-PLL/SF(Y,S)-PGA silk ionomer shells (a) and highly PEGylated double brush graft copolymer (SF(Y,S)-PLL-*g*[9]-PEG/SF(Y,S)-PGA) shells (b) in comparison to control nonencapsulated cells (c) imaged with confocal (i), SEM (ii) and AFM (iii) microscopy (from 1 μm^2 surface area). Z-range in (iii) is 200 nm.**

In contrast, hydrogen-bonded shells based on PEGylated double-brush graft silk copolymer and protonated anionic silk ionomer showed highly stable colloidal suspension of cells-in-shells structures, demonstrating the cell-repellent character of highly PEGylated coatings (Figure 5b, 6b). High grafting density (g = 9) of long hydrated chains of PEGs (M_w = 5 kDa) promoted extended truly "bottle brush" conformation of PEGs along the poly lysine chains as well as more extended conformations of the backbone of silk macromolecules that forms even, smooth LbL films.[68] Interestingly, the immobilization of functionalized silk protein shells (regardless of the nature of the interactions involved in the shell assembly) at cell surfaces provided structural robustness for the encapsulated cells against external perturbations (high or low pressure, shear stresses), as evidenced from SEM micrographs. Cells encapsulated in these brush protein shells had distinct rod-shape appearance while maintaining the internal cell volume characteristic to the natural presence of cells. In contrast, nonencapsulated cells appeared collapsed under high vacuum during SEM imaging (Figures 5c, 6c).

Effect of assembling low charge density silk polyelectrolyte shells (SF(S)-PLL/SF(S)-PGA) on aggregation of cells had no effect with respect to the cell type (for the sake of the simplicity, we only included results for *B. subtilis*, as the best representative candidate). Cell cluster sizes reduced to 10−30 μm (Figure 7). Additionally, significantly lower surface microroughness was observed with AFM imaging in comparison to the high charge density silk polyelectrolytes. In this case, cells aggregation was reduced due to the low grafting density and shorter charged amino acid side chains. Furthermore, assembly of silk shells from brush-like PEGylated block copolymers further reduces aggregation of cells-in-shells assemblies (below 10 μm) due to hydrophilic nature of terminal PEG chains and resulted in smoother LbL shells. Apparently, even relatively short PEG side chains (n = 20) attached to the backbone of the silk molecules through short lysine groups (n = 10) promoted more extended conformation of silk macromolecules that contributed to the formation of stable shells assembled *via* complex nonspecific interactions.

AFM assessment of the surface microroughness (root-mean-square, Rq) in the dry collapsed state (calculated from 1 μm^2 surface area in AFM images) confirmed significant differences in the Rq values with respect to the nature of the silk protein shells and the type of cells ($p < 0.01$) (Table 2). Flattened bacterial cells (*B. subtilis*) had a surface roughness of Rq = 3.1 ± 0.8 nm (after fixation and drying), while rougher cells (*E. coli*) had a surface roughness of Rq = 5.4 ± 0.8 nm. Higher Rq values were observed for highly charged silk polyelectrolytes assembled on both types of bacterial cells with Rq = 14.8 ± 3 nm for *B. subtilis* and 19.5 ± 4.1 nm for and *E. coli* cells. In contrast, pure hydrogen-bonded shells

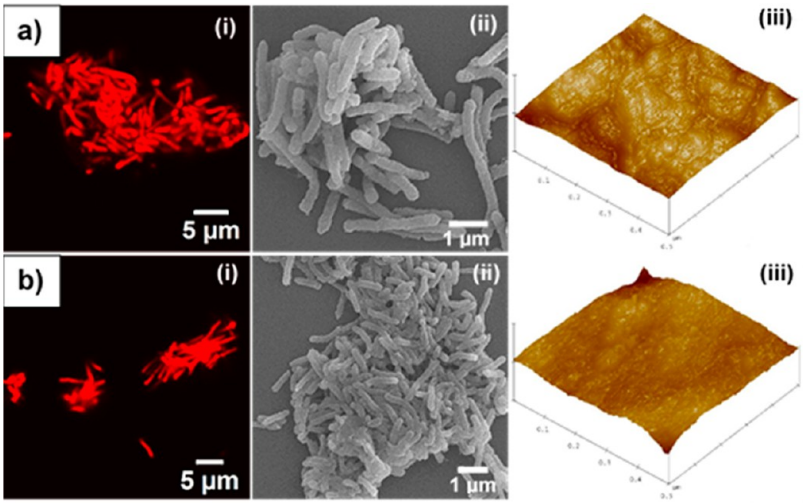

Figure 7. *B. subtilis* cells encapsulated in 4 bilayers of *low charge* density silk polyelectrolyte SF(S)-PLL/SF(S)-PGA shells (a) and PEGylated silk brush-like block copolymers (SF(S)-PLL-*b*-PEG/SF(S)-PGA) shells (b) imaged with confocal (i), SEM (ii) and AFM (iii) microscopy (from 1 μm^2 surface area). Z-range in (iii) is 200 nm.

TABLE 2. Surface Microroughness (Root-Mean-Square, Rq, nm) of Dried Bacterial Cells Encapsulated in 4 Bilayered Shells Assembled from Different Types of Silk Polyelectrolyte Brushes[a]

cell type/silk shell	bare surface	SF(Y,S)-PLL/SF(Y,S)-PGA	SF(Y,S)-PLL-*g*[9]-PEG/SF(Y,S)-PGA	SF(S)-PLL/SF(S)-PGA	SF(S)-PLL-*b*-PEG/SF(S)-PGA
E. coli	5.4 ± 0.8	19.5 ± 4.1	6.1 ± 1.2	9.6 ± 1.5	7.4 ± 1.1
B. subtilis	3.1 ± 0.8	14.8 ± 3.0	4.4 ± 1.3	7.5 ± 1.1	5.6 ± 0.8

[a] Images (from 1 μm^2 surface area) have been processed by build-in software. Experimental values are represented as means ± SD, $n = 15$.

demonstrated significantly smoother film structures with Rq = 4.4 ± 1.3 nm and 6.1 ± 1.2 nm for *B. subtilis* and *E. coli* cells, respectively. During encapsulation with low charge density silk polyelectrolyte shells, roughness increased to Rq = 7.5 ± 1.1 nm and Rq = 9.6 ± 1.5 nm for *B. subtilis* and *E. coli* cells, accordingly, whereas for PEGylated block copolymer silk shells the roughness decreased to Rq = 5.6 ± 0.8 nm and Rq = 7.4 ± 1.1 nm, which is still 25% higher than corresponding values for pure hydrogen-bonded silk shells.

Viability of Silk-Encapsulated Microbial Cells. Viability of cells encapsulated in silk polyelectrolyte shells was assessed with two toxicity assays to study the effect of silk polyelectrolytes (Figures 8, S5) (see Methods). Bioreduction of resazurin was used immediately after the encapsulation to assess the susceptibility of bacterial cells to the processing conditions and the exposure to silk copolymers. The results were confirmed with a formazan-based cell proliferation assay (MTT) after incubation in cell culture medium for 24 h. The MTT assay gave 10% higher viability values compared to the resazurin-based assay due to the difference in time exposure and distinct nature of the two assays.[69] Consistently, *B. subtilis* cells demonstrated on average 5−10% higher viability than *E. coli* cells, in spite of the more receptive nature of their cell walls to chemical agents.[66,70]

Cells encapsulated in four bilayered LbL shells using highly charged silk polyelectrolytes (SF(Y,S)-PLL/SF(Y,S)-PGA)$_4$ showed reduced viability of 13−16%

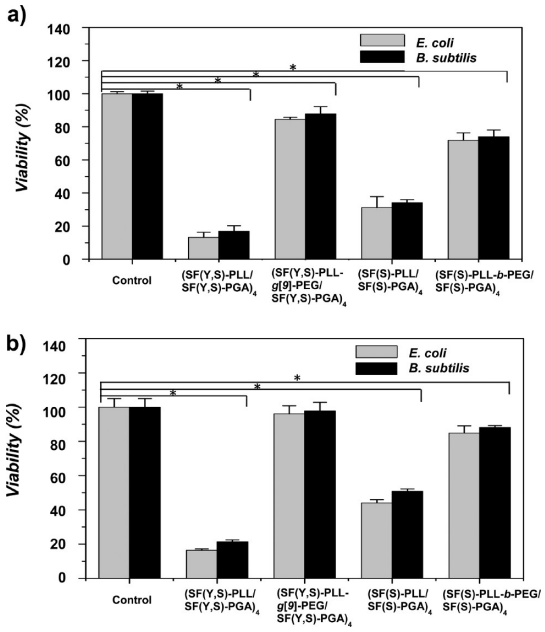

Figure 8. Comparison of viability for two types of bacterial cells encapsulated in *high charge* density (SF(Y,S)-PLL/SF(Y,S)-PGA)$_4$ silk polyelectrolyte shells; highly PEGylated double brush graft copolymer (SF(Y,S)-PLL-*g*[9]-PEG/SF(Y,S)-PGA)$_4$ shells; *low charge* density (SF(S)-PLL/SF(S)-PGA)$_4$ silk polyelectrolyte shells; and PEGylated brush-like silk block copolymer (SF(S)-PLL-*b*-PEG/SF(S)-PGA)$_4$ shells as the result of intermolecular interactions. Viability was assessed with resazurin-based assay after 2 h of incubation (a) and MTT-based test after 24 h of incubation (b). Experimental values are represented as means ± SD, $n = 3$. Paired *t* test, $^*p < 0.01$.

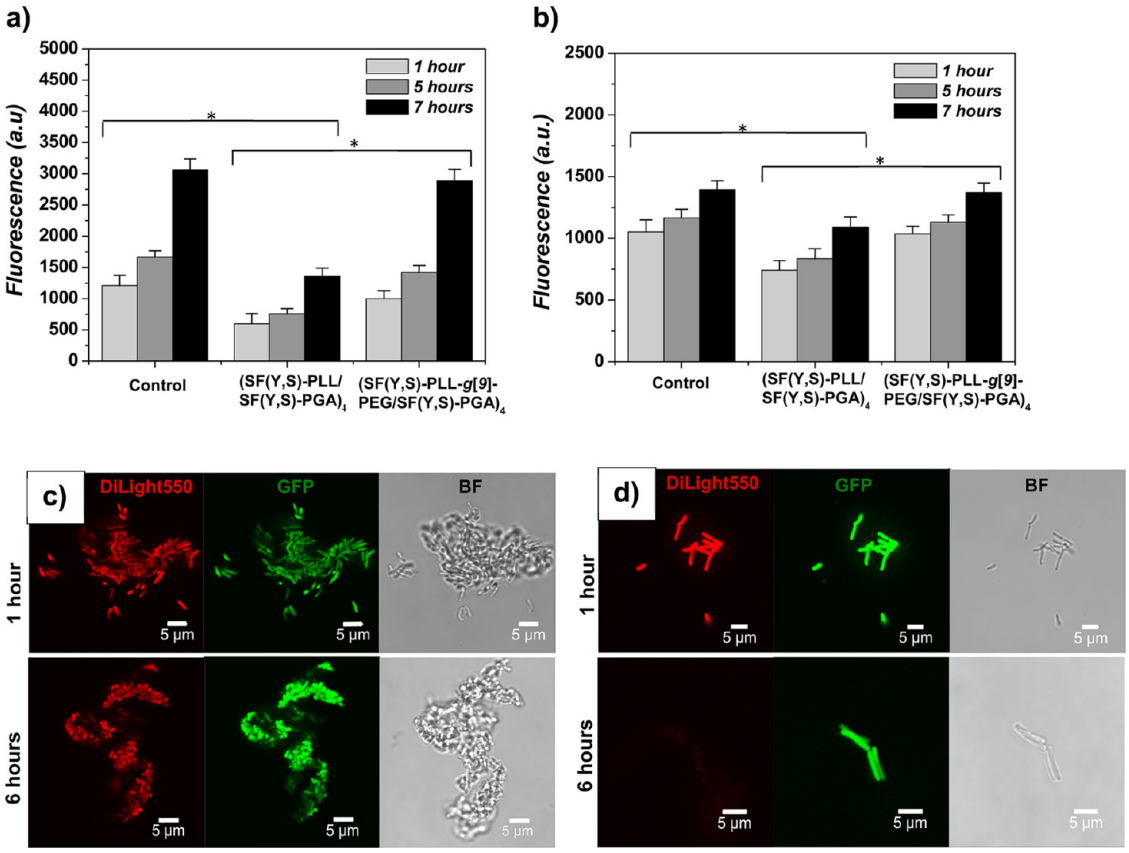

Figure 9. Kinetics of GFP expression in *E. coli* (a) and *B. subtilis* (b) bacterial cells encapsulated in *high charge* density silk ionomer (SF(Y,S)-PLL/SF(Y,S)-PGA)$_4$ shells and highly PEG-grafted double-brushes (SF(Y,S)-PLL-*g*[9]-PEG/SF-PGA)$_4$ shells. Experimental values are represented as mean ± SD, $n = 6$. Paired *t* test, $*p < 0.05$. Representative confocal images of *B. subtilis* cells encapsulated in polyelectrostatic (SF(Y,S)-PLL/SF(Y,S)-PGA)$_4$ (c) and hydrogen-bonded (SF(Y,S)-PLL-*g*[9]-PEG/SF(Y,S)-PGA)$_4$ (d) shells after incubation in cell culture medium supplemented with 5 mM of theophylline for 1 and 6 h. Left columns in (c) and (d) represent fluorescently labeled shells (DiLight550); middle columns, GFP production by cells; and right columns, bright field (BF) images of the cells.

(for *E. coli* cells) and 17−21% (for *B. subtilis* cells) (Figure 8a,b). As was reported, high charge density polycations can elicit cytotoxicity due to nonspecific formation of pores in the plasma membrane of eukaryotic cells that can depend on the size and conformation of the polymers used for the cell coatings.[45] Similarly, cationic polymers are well-documented in having a general bacterial-static effect due to the charge interaction with the cell membranes.[71,72] Bacterial cells are known for their resilience to external perturbations in the local environment, including minor disruptions in the plasma membrane, and their ability to denature nonessential proteins or membrane lipids. The fact that high charge density silk polyelectrolyte shells have significant effect on metabolic behavior and inhibition of growth (at least within the first 24 h) confirmed the adverse effects of conventional silk polyelectrolytes with high molecular weight of polyamino acid side chains on bacterial microorganisms.

In contrast, PEGylated double-brush graft silk copolymer SF(Y,S)-PLL-*g*[9]-PEG and its highly protonated SF(Y,S)-PGA counterpart had no effect on microbial activity, making these shells cytocompatible. Both types of bacteria encapsulated in hydrogen-bonded (SF(Y,S)-PLL-*g*[9]-PEG/SF(Y,S)-PGA)$_4$ shells demonstrated viability of 85−96% (for *E. coli*) and 88−98% (for *B. subtilis*), indicating adverse effects of polycationic charges on cellular biocompatibility (Figure 8a,b). Indeed, bacterial cells encapsulated in 4-bilayered LbL shells using silk ionomers with low charge density have already demonstrated viability of 31−45% for *E. coli* and 34−54% for *B. subtilis* cells, respectively, which is significantly higher as compared to silk polyelectrolytes of high charge density (paired *t* test, $p < 0.01$) (Figure 8a,b). Cells encapsulated in silk shells assembled with brush-like PEGylated block copolymers had increased the viability to 71−84% for *E. coli* and 74−88% for *B. subtilis*, respectively, emphasizing the positive effect of decreasing the charge density of polycations with PEG grafts on improved cell viability. Hence, by lowering the charge density of silk polyelectrolytes (either by reducing degree of derivation of backbones with polycations and/or decreasing molecular weight of these side chains) viability of encapsulated cells can be improved. This is consistent with

previous reports on an inverse correlation between M_w and charge density with cell toxicity.[45,73]

The cytotoxic effect of polycations can also be significantly reduced by adsorbing buffer layers to shield the cell surface from conformational changes induced by amino groups of polycations. Bacterial cells primed with two SF layers prior to the adsorption of silk polyelectrolytes showed significantly higher viability of 51−60% for *E. coli* cells and 56−63% for *B. subtilis* cells, respectively compared to low charge density silk ionomers (Figure S5). These results suggest that the toxicity originates during direct interaction of polycations with cell membranes as a result of enhanced interfacial interactions with amino-groups.

Function of Encapsulated Riboswitch-Hosted Cells As Biosensors. In our study we utilized recombinant bacteria engineered with synthetic riboswitch constructs.[74,75] The riboswitch is a genetic construct composed of two structural domains: an aptamer domain that binds to a small molecule and an expression platform that controls the expression of a downstream gene *via* conformational changes, which are induced by the ligand (target analyte) binding to the aptamer. Cell-based biosensors preprogrammed with engineered reporter-gene constructs offer exceptional specificity, controlled response and significant signal amplification, which can be used for detection, identification and tracking the molecules of interest.[76]

The ability of cell-based biosensors to function and respond to the analyte after encapsulation provides important information regarding the cytocompatibility of functionalized silk brush coatings. Depending on the chemical composition of the shells and the type of cellular construct associated with the analyte recognition in recombinant cells, encapsulated cells responded differently to the presence of analyte (theophylline). Figure 9a,b represents kinetics of GFP expression during incubation of encapsulated cells (both *E. coli* (a) and *B. subtilis* (b)) in cell culture medium supplemented with 5 mM theophylline. Importantly, analytical recognition was cell-specific. *E. coli* was the most efficient cell platform for processing and activating the reporter gene, as a part of the riboswitch construct, due to higher levels of fluorescence intensity and more dynamic signal amplification (exponential growth) of the intensity within the course of study (Figure 9a,b).

Overall, regardless of the cell type, cells encapsulated in high charge density silk polyelectrolytes had lower intensity of GFP appearance as compared to more cytocompatible hydrogen-bonded shells based upon brush-like graft silk backbones with a high degree of grafting density of PEGs (Figure 9a,b). The apparent difference in fluorescence intensity was significant at least during the first 7 h of monitoring fluorescence (paired t test, $p < 0.01$). This trend was not surprising due to the fact that strong polycationic polymers (regardless of their nature) impose cytotoxicity to the functionalized cells, which correlates linearly with the graft density of charged groups and the length of the polycationic side chains.[45] In our case, cells encapsulated in silk polyelectrolyte shells assembled through electrostatic interactions with high-charge density silk polymers had significantly reduced viability, and as a result, low fluorescence intensities. In contrast, cytocompatible hydrogen-bonded shells assembled with double-brushes made from highly PEGylated graft silk copolymers supported cell activity and demonstrated induced GFP fluorescence comparable to nonencapsulated cells with the highest activity.

With respect to the stability of these engineered shells, cells encapsulated in different types of shells were stable as colloidal suspensions for prolonged period of time (up to 3−4 months) if kept in aqueous solutions at ambient conditions. During warming-up, shells did not show any degradation for several hours; however, hydrogen-bonded shells started to deteriorate after 4−5 h during incubation at 37 °C in concentrated cell medium (rich in amino acids and salts) under vigorous agitation (220 rpm). The remnants of the fluorescently labeled red shells were observed only after 6 h of incubation (Figure 9d). In contrast, during a comparable time frame, electrostatically bound (both with high and low charge density) and brush-like PEGylated silk block copolymer shells demonstrated significant stability toward degradation as red fluorescence associated with labeled shells overlapped with cells producing GFP (Figure 9c). Hence, minor inclusions of polycationic components of small molecular weight can promote the stability of LbL shells and restrict the cell growth and binary division.

Bacteria encapsulated in silk polyelectrolyte shells of low charge density and shorter PEG side chains demonstrated higher levels of GFP fluorescence intensity in comparison to high charge density silk polyelectrolyte shells (Figure 10). Higher intensities were correlated with the higher viability rates emphasizing the negative effect of high charge density polycationic electrolytes on functionality of the cells. Consistently, if cells were primed with two layers of silk fibroin ($(SF)_2$) prior to encapsulation with low charge density polyelectrolytes ($(SF)_2$/SF(S)-PLL/SF(S)-PGA)$_3$ shells), the capacity of cells to respond to the analyte was not inhibited (Figure S6). The fluorescence from GFP-producing cells encapsulated in such shells showed comparable levels of intensity in cells encapsulated with brush-like PEG-block silk copolymers. Notably, *E. coli* cells recovered faster and had higher intensities of GFP expression in response to the effector cues compared to *B. subtilis* due to higher efficiency of theophylline riboswitch in *E. coli* cells.[74]

The viability results were consistent with cell functioning in terms of the potential of cells to respond to

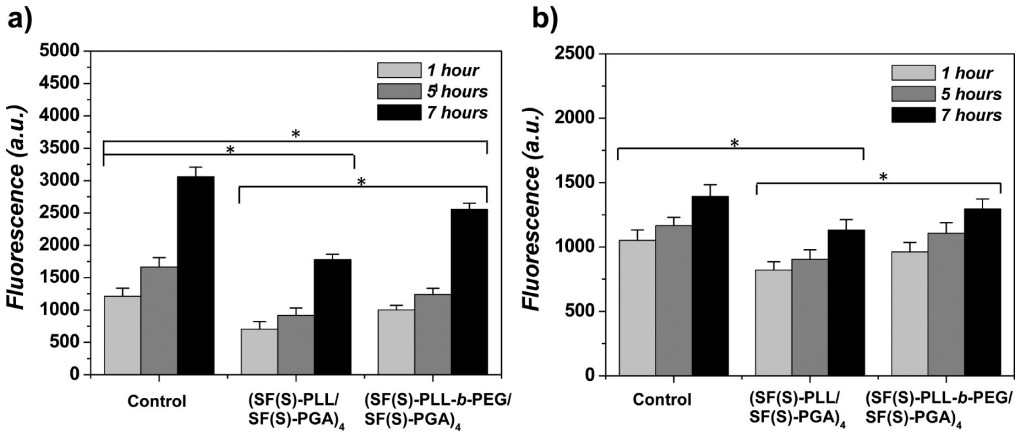

Figure 10. Kinetics of GFP expression in *E. coli* (a) and *B. subtilis* (b) cells encapsulated in *low charge* density (SF(S)-PLL/SF(S)-PGA)$_4$ silk polyelectrolyte shells and brush-like PEG block (SF(S)-PLL-*b*-PEG/SF(S)-PGA)$_4$ silk copolymer shells. Experimental values are represented as means ± SD, $n = 6$. Paired *t* test, $*p < 0.05$.

the target analyte, which binds to the aptamer domain and turns "ON" the expression of GFP.[77] The cell function studies confirmed that the highly porous nanoshells (open pores of tens of a nanometer)[27,28] did not restrict the diffusion of theophylline, and the ability of cells to respond to the presence of analyte was more a factor of the polycationic component of the shells. Cationic silk polyelectrolytes and subsequently electrostatically driven assembly of silk shells played a major role in nominal production of GFP signal as the cells had to recover first from transient destruction in the cell membrane caused by conformational changes in polylysine chains of silk polycationic grafts. However, the recovery of bacterial cells was much faster compared to any eukaryotic cells,[26] which explains the efforts on engineering the cell-based sensors using synthetic biology principles in bacteria.[78,79] Within an hour cells were able to activate the fluorescent marker and accumulate GFP to high intensity levels.

From the perspective of cell-based devices, rapid response from cells individually confined in ultrathin and permeable shells is usually required for biosensing applications (cell-based sensors, bioreactors, or microfluidic channels). Such shells can contribute to the long-term stability and performance of cell-based devices.[80] On the contrary, the formation of cell clusters with polymeric material can found more applications in the field of clinical medicine, ecology, microbiology and geotechnical engineering, where matrix-enclosed 3D communities can be studied in biofilm science to prevent infectious diseases, or aid in soil biocementation, disinfection, water and fuel treatments.[81,82] Hence, ability to render the spatial organization of cells in the form of aggregates or have them individually coated with organic/inorganic material can be valuable means for controlling the survivability, growth rate and gene transcription of encapsulated cells.

CONCLUSIONS

In conclusion, we demonstrated that by tailoring the chemical design of regenerated fibroin silk macromolecule with variable molecular weight, grafting density and architecture of amino acids/PEG chains, significant morphological and functional capabilities of cells encapsulated in such brushes can be acquired. The molecular weight of poly amino acids, molecular weight and degree of PEG grafting were varied in order to assess the formation of cytocompatible and robust LbL shells on two types of Gram bacteria. The viability and activity of encapsulated cells were inversely related to the charge density and molecular weight of polycationic amino acid silk grafts. In contrast, because of the strong correlation between high viability/function of cells and molecular weight/grafting density of PEG side chains, highly PEGylated silk brushes assembled *via* hydrogen bonding with protonated polyanionic silk macromolecules demonstrated the highest cytocompatibility (up to 98%) and promoted single-cell encapsulation with distinct antifouling appearance.

Distinct chemical signatures of bacterial envelopes as templating substrates in combination with high charge density and length of ionized silk polycationic side chains played a significant role in coarsening the surface of encapsulated cells and promoting the clustering of cells. Because of the presence of long polysaccharide chains at the surface of *E. coli* cells, adsorption of bulky silk amino acid grafts of high charge density resulted in the formation of large cell aggregates. In contrary, structurally more flat cell envelopes of *B. subtilis* cells demonstrated significantly reduced agglomeration of cells during LbL encapsulation with the same silk amino acid grafts. Furthermore, during adsorption of high charge density silk polyelectrolytes, conformational changes in silk brushes induced by long charged side chains promoted

globular appearance of proteins through extensive intermixing of side chains, at which point individual nanoparticles can be formed.

Stable colloidal suspensions (under ambient conditions) of individually coated, active cells can find potential for flow-based devices, such as microfluidic channels or bioreactors. On the other hand, induced clustering of cells by using small inclusions of positively charged amino acids terminated by hydrophilic molecules is highly favorable for cells survival and prolonged circulation, which can be beneficial in the field of clinical medicine, ecology, or microbiology. Tailoring the charge density of brush-like silk polyelectrolytes with proper grafting density of PEG side chains can be useful for synthesis of proper natural polymer derivatives that provide necessary robustness and cytocompatibility with controlled spatial arrangement of cells and their aggregates, which can be rewarding for biosensor-related and broader biomedical applications.

METHODS

Materials. Monobasic sodium phosphate (NaH_2PO_4), phosphate buffer saline (PBS), theophylline, osmium tetroxide (4%), glutaraldehyde, poly(L-lysine) hydrobromide (PLL) ($M_w \leq$ 15 000 Da), poly(L-glutamic acid) sodium salt (PGA) ($M_w \leq$ 15 000 Da), methoxypolyethylene glycol propionic acid N-succinimidyl ester (mPEG-SPA) (M_w = 5000 Da) were purchased from Sigma-Aldrich (St. Louis, MO). Monodispersed poly-L-lysine hydrochloride (PLL_{20}) (M_w = 3000 Da), methoxy-poly(ethylene glycol)-*block*-poly(L-lysine hydrochloride) (PLL_{10}-*b*-PEG_{22}) (M_w = 2600 Da) and poly(L-glutamic acid sodium salt (PGA_{20}) (M_w = 3000 Da) amino acids were purchased from Alamanda Polymers (Huntsville, AL). Cross-linker, 1-ethyl-3-[3-(dimethylamino) propyl] carbodiimidehydrochloride (EDC), was purchased from Thermo Fisher Scientific (Rockford, IL).

Synthesis of Silk Ionomers. High charge density silk ionomers (SF(Y,S)-PGA and SF-(Y,S)-PLL) were obtained using our previously published methods.[48] In particular, silk fibroin (SF) solution was obtained by extraction from *Bombyx mori* cocoons according to established procedures.[83] Subsequently, SF structure was enriched in carboxyl groups by the diazonium coupling to tyrosine (Y) and serine (S) side chains of the protein. The obtained carboxy-silk (SF(Y,S)-COOH) was then covalently conjugated with PLL or PGA *via* EDC chemistry to obtain high charge density SF(Y,S)-PLL and SF(Y,S)-PGA silk ionomers.[48] Low charge density SF(S)-PLL and SF(S)-PGA silk ionomers were obtained by grafting PLL_{20} or PGA_{20} to carboxyl-modified serine (S) residues of 5 min-boiled SF(S) by a similar set of reactions.

PEG-Grafted Brushes of Different Architecture. Graft (*g*) double-brush copolymer silk protein SF(Y,S)-PLL-*g*[*D*]-PEG was synthesized by conjugation mPEG-SPA to PLL side chains of a high charge density SF(Y,S)-PLL silk ionomer with 4 mol % and 9 mol % degree of grafting ratio, designated as *D*. In more detail, SF(Y,S)-PLL (90 mg, 2 mL) was dissolved in phosphate buffer (pH 8.5) and slowly added to PBS (1X, 2 mL, pH 8.5) containing mPEG-SPA (70 mg) or mPEG-SPA (150 mg) to produce PEG brushes of 4 or 9 mol % grafting degree, correspondingly. The reaction was continued for 18 h at room temperature in the dark, then transferred to a Slide-A-Lyzer dialysis cassette (15 mL, MWCO = 10 kDa) (Thermo Scientific) and dialyzed against PBS (pH 8.5), then subsequently lyophilized.

Block copolymer brush protein SF(S)-PLL-*b*-PEG was synthesized by conjugation PLL_{10}-*b*-PEG_{22} block polymer to carboxyl-modified serine residues of a 5 min boiled SF(S)-COOH according to the same procedure for obtaining low charge density silk ionomers. All polymers have been analyzed by ^1H NMR using D_2O as a solvent. ^1H NMR spectra were taken on a Bruker DRX 400 spectrometer operating at 400 MHz.

Recombinant Bacterial Cells. BL21 *E. coli* and 1012 WT *B. subtilis* cells (from Novagen) were transformed with plasmids containing synthetic riboswitch constructs. Theophylline riboswitch (clone 12.1)[84,85] in BL21 *E. coli* cells was placed upstream of the sequence encoding a new fluorescent protein (GFPa1) from *Amphioxus*[86] in pSAL plasmid (pSAL:RS12.1GFPa1His). In 1012 WT *B. subtilis* cells, theophylline synthetic riboswitch[74] was placed upstream of superfolder GFP encoding sequence[87] in pHT01 plasmid vector (pHT01:RSE_sfGFP). Bacterial cells were cultured in Luria−Bertani (LB) broth supplemented with 50 μg/mL of ampicillin (for *E. coli*) and 10 μg/mL of chloramphenicol (for *B. subtilis*). Cells were grown at 37 °C in a shaker incubator (New Brunswick Scientific) with 220−240 rpm to bring them to an early exponential phase (OD_{600} = 0.3−0.5 au based on a 0−2 scale) (GE cell calculator). Activation of the riboswitch was induced with 5 mM theophylline (DMSO), and fluorescence was visualized on the confocal microscope (Zeiss LSM510 system).

LbL Assembly of Silk Ionomer Shells on Bacterial Cells. Prior to encapsulation cells were harvested from LB medium in 15 mL centrifuge tubes by centrifugation (3000 rpm for 2 min) and extensive washing with PBS (3 × 15 mL). Deposition of electrostatically bound shells of high and low charge density silk ionomers started from SF(Y,S)-PLL or SF(S)-PLL (1 mg/mL, 0.05 M NaH_2PO_4, pH 6) followed by SF(Y,S)-PGA or SF(S)-PGA (1 mg/mL, 0.05 M NaH_2PO_4, pH 6) until the desired number of bilayers has been reached. Partially screened electrostatic shells were assembled by incubation in the solution of SF(S)-PLL (1 mg/mL, 0.05 M NaH_2PO_4, pH 6) followed by incubation in SF(S)-PGA (1 mg/mL, 0.05 M NaH_2PO_4, pH6) solution until the desired number of bilayers has been reached. Hydrogen-bonded shells were assembled by incubation cells in the solution of SF(Y,S)-PLL-*g*[9]-PEG (1 mg/mL, 0.05 M NaH_2PO_4, pH 4) followed by incubation in SF(Y,S)-PGA (1 mg/mL, 0.05 M NaH_2PO_4, pH 4) solution. Cells were incubated in 1 mL of protein solution on a rotating stage (20 rpm) for 10 min followed by centrifugation (3000 rpm for 2 min) and washing in phosphate buffer (0.05 M, pH 6) (3 × 2 mL). Encapsulated cells were stored at 4 °C unless further studies on cell viability, activation of riboswitch or zeta-potential measurements were performed.

Labeling of Silk with DyLight Fluorescent Dye. DyLight antibody labeling kit containing DiLight550 NHS-ester dye was purchased from Thermo Scientific (Pierce Biotechnology, Rockford, IL). Conjugation of dye to SF(S,Y)-PLL (2 mg/mL, 50 mM sodium borate, pH 8.5) was performed according to the manufacturer's protocol. Fluorescently labeled silk (0.5 mg/mL, 0.05 M NaH_2PO_4, pH 7) was allowed to absorb as a last layer on each type of silk shells.

Ellipsometry. Measurements were obtained on an M-2000U spectroscopic ellipsometer (Woolam). Silk films were deposited on freshly cleaned silicon wafers from aqueous solutions of appropriate pH (1 mg/mL, 0.05 M NaH_2PO_4) using the dip-assisted method. Deposition of different types of silk films was performed for 10 min followed by washing in the appropriate pH phosphate buffer (0.05 M) (2 × 5 mL).

Cytotoxicity Assays. MTT and resazurin-based cytotoxicity assays tests (three replicates per each test) were performed to assess effect of the coatings and encapsulation procedures on the cells.[88] Resazurin-based test was performed immediately after encapsulation according to manufacturer's protocol (Biotium, Hayward, CA). Fluorescence from rezarufin was measured at λ_{em} = 585 nm (λ_{ex} = 560 nm) on a spectrofluorophotometer (Shimadzu RF 5301 PC) after incubation for 2 h. The mitochondrial MTT assay (Trevigen, Inc. Gaithersburg, MD) was used to assess cell membrane integrity and cellular ATP levels. The concentration of solubilized formazan produced during

24 h incubation of cells in cell medium was determined by absorbance at 570 nm on (Schimadzu UV-2450) spectrophotometer.

Zeta-Potential. Measurements were performed to determine the surface charge of the coatings after deposition of each layer. Measurements were obtained on Zetasizer Nano-ZS equipment (Malvern) using clear disposable polystyrene Zeta-potential cuvettes. After deposition of each layer cells were extensively washed with appropriate phosphate buffer (0.05 M NaH_2PO_4) (3 × 2 mL) followed by washing with Nanopure water (1 × 2 mL). Aliquots of cells sample (100 μL) were combined with autoclaved Nanopure water (900 μL) to obtain 1 mL volume. Each measurement was collected at ambient conditions (25 °C) by averaging three independent measurements of 35 subruns using the Smoluchowski model.

Scanning Electron Microscopy. SEM was performed on Hitachi-S-3400-II system at an operating voltage of 10 keV. Samples (20 μL of cell suspensions) were drop casted on silicon wafers, air-dried and sputtered with ~2 nm gold film. Prior to imaging, cells were fixed with glutaraldehyde aqueous solution (4% w/v) for 60 min, washed with autoclaved DI water (4 × 2 mL) and dehydrated stepwise with 25, 50, 75 and 100% of ethanol. SEM scanning was first performed on a large area (100 × 100 μm^2) of cells (at least 200), then zoomed in to show individual clusters of cells or group of single cells followed by imaging single cells.

Atomic Force Microscopy. AFM was performed on a Dimension-3000 (Digital Instruments) microscope in the "'light'" tapping mode (100−500 kHz resonant frequency) at 90° scanning direction using silicon V-shape cantilevers having a spring constant of 46 N/m according to usual procedure.[89] Fixed samples (gluteraldehyde, aqueous 4% w/v) were drop casted on silicon wafer and air-dried before AFM scanning. AFM imaging was conducted on encapsulated and nonencapsulated (control) cells (at least 4−5 cells), starting from 20 × 20 μm^2 area scan, and progressively zooming in to scan a target 1 × 1 μm^2 surface area. In order to determine mean root-mean-square (Rq) surface roughness, 1 μm^2 height scans (from 4 to 5 cells) were processed with DI-3000 software.

Transmission Electron Microscopy. TEM imaging of encapsulated and nonencapsulated Gram-positive bacteria (*B. subtilis*) cells was performed on Hitachi H-7600 Transmission Electron microscope. Prior to imaging, cells were stained with osmium tetroxide (1%, o.1 M PBS), washed with PBS (3 × 1 mL) and dehydrated using graded series of athanol (50, 70, 80, 90 and 100%). Following the dehydration cells were imbedded in white resin (1:1 ratio, 100% ethanol) and sliced with microtome.

Confocal Laser Scanning Microscopy. CLSM images of microbial cells encapsulated in different composition of shells were obtained on a Zeiss LSM 510 system equipped with Ar laser and He−Ne lases). Emission from GFPa1 was visualized with 515 nm band-pass filter (excitation at 488 nm). Fluorescently labeled shells were imaged by excitation at 543 nm and visualized with 560−590 nm band-pass filter.

Statistical Analysis. Data are expressed as means ± standard deviation, with variable number of repeats (n) for each experimental group. Statistical analysis was performed on all samples using paired t test to evaluate significant differences between groups with $p < 0.05$ or $p < 0.01$.

Conflict of Interest: The authors declare no competing financial interest.

Acknowledgment. The study was supported by grants FA9550-14-1-0269 and FA9550-09-1-0162 (BIONIC Center) from Air Force Office of Scientific Research and NSF CBET-1402712. We acknowledge Dr. O. Shchepelina for synthesis of some PEG graft polymers, Dr. P. Ledin for the help with chemical structure drawings, Ren Geryak for valuable discussion, and Rachael McGuire for help with cell encapsulation. TEM images were obtained by P. F. Lloyd (UES, Inc.).

Supporting Information Available: ^{1}H NMR spectra of silk copolymers, viability and kinetics of GFP expression of bacteria encapsulated in low-charge silk polyelectrolytes initially primed with pure silk fibroin. This material is available free of charge *via* the Internet at http://pubs.acs.org.

REFERENCES AND NOTES

1. Fuqua, W.; Winans, S.; Greenberg, E. P. Quorum Sensing in Bacteria: the LuxR-LuxI Family of Cell Density-Responsive Transcriptional Regulators. *J. Bacteriol.* **1994**, *176*, 269–275.
2. Waters, C. M.; Bassler, B. L. Quorum Sensing: Cell-to-Cell Communication in Bacteria. *Annu. Rev. Cell Dev. Biol.* **2005**, *21*, 319–346.
3. Fux, C. A.; Costerton, J. W.; Stewart, P. S.; Stoodley, P. Survival Strategies of Infectious Biofilms. *Trends Microbiol.* **2005**, *13*, 34–40.
4. Hall-Stoodley, L.; Costerton, J. W.; Stoodley, P. Bacterial Biofilms: from the Natural Environment to Infectious Diseases. *Nat. Rev. Microbiol.* **2004**, *2*, 95–108.
5. Miller, M. B.; Bassler, B. L. Quorum Sensing in Bacteria. *Annu. Rev. Microbiol.* **2001**, *55*, 165–199.
6. Hense, B. A.; Kuttler, C.; Müller, J.; Rothballer, M.; Hartmann, A.; Kreft, J. U. Does Efficiency Sensing Unify Diffusion and Quorum Sensing? *Nat. Rev. Microbiol.* **2007**, *5*, 230–239.
7. Donlan, R. M.; Costerton, J. W. Biofilms: Survival Mechanisms of Clinically Relevant Microorganisms. *Clin. Microbiol. Rev.* **2002**, *15*, 167–193.
8. Hall-Stoodley, L.; Costerton, J. W.; Stoodley, P. Bacterial Biofilms: from the Natural Environment to Infectious Diseases. *Nat. Rev. Microbiol.* **2004**, *2*, 95–108.
9. Carnes, E. C.; Lopez, D. M.; Donegan, N. P.; Cheung, A.; Gresham, H.; Timmins, G. S.; Brinker, C. J. Confinement-Induced Quorum Sensing of Individual *Staphylococcus aureus* Bacteria. *Nat. Chem. Biol.* **2009**, *6*, 41–45.
10. Novick, R. P.; Geisinger, E. Quorum Sensing in Staphylococci. *Annu. Rev. Genet.* **2008**, *42*, 541–564.
11. Balkundi, S. S.; Veerabadran, N. G.; Eby, D. M.; Johnson, G. R.; Lvov, Y. M. Encapsulation of Bacterial Spores in Nanoorganized Polyelectrolyte Shells. *Langmuir* **2009**, *25*, 14011–14016.
12. Fakhrullin, R. F.; Zamaleeva, A. I.; Minullina, R. T.; Konnova, S. A.; Paunov, V. N. Cyborg Cells: Functionalisation of Living Cells with Polymers and Nanomaterials. *Chem. Soc. Rev.* **2012**, *41*, 4189–4206.
13. Drachuk, I.; Gupta, M.; Tsukruk, V. V. Biomimetic Coatings to Control Cellular Function through Cell Surface Engineering. *Adv. Funct. Mater.* **2013**, *23*, 4437–4453.
14. Hong, D.; Park, M.; Yang, S. H.; Lee, J.; Kim, Y. G.; Choi, I. S. Artificial Spores: Cytoprotective Nanoencapsulation of Living Cells. *Trends Biotechnol.* **2013**, *31*, 442–447.
15. Fakhrullin, R. F.; Lvov, Y. M. Face-Lifting" and "Make-Up" for Microorganisms: Layer-by-Layer Polyelectrolyte Nanocoating. *ACS Nano* **2012**, *6*, 4557–4564.
16. Dzamukova, M. R.; Zamaleeva, A. I.; Ishmuchametova, D. G.; Osin, Y. N.; Kiyasov, A. P.; Nurgaliev, D. K.; Ilinskaya, O. N.; Fakhrullin, R. F. A Direct Technique for Magnetic Functionalization of Living Human Cells. *Langmuir* **2011**, *27*, 14386–14393.
17. Krol, S.; Del Guerra, S.; Grupillo, M.; Diaspro, A.; Gliozzi, A.; Marchetti, P. Multilayer Nanoencapsulation. New Approach for Immune Protection of Human Pancreatic Islets. *Nano Lett.* **2006**, *6*, 1933–1939.
18. Yang, S. H.; Ko, E. H.; Choi, I. S. Cytocompatible Encapsulation of Individual Chlorella Cells within Titanium Dioxide Shells by a Designed Catalytic Peptide. *Langmuir* **2011**, *28*, 2151–2155.
19. Yang, S. H.; Ko, E. H.; Jung, Y. H.; Choi, I. S. Bioinspired Functionalization of Silica-Encapsulated Yeast Cells. *Angew. Chem., Int. Ed.* **2011**, *50*, 6115–6118.
20. Drachuk, I.; Shchepelina, O.; Lisunova, M.; Harbaugh, S.; Kelley-Loughnane, N.; Stone, M.; Tsukruk, V. V. pH-Responsive Layer-by-Layer Nanoshells for Direct Regulation of Cell Activity. *ACS Nano* **2012**, *6*, 4266–4278.
21. Yang, S. H.; Kang, S. M.; Lee, K. B.; Chung, T. D.; Lee, H.; Choi, I. S. Mussel-Inspired Encapsulation and Functionalization of Individual Yeast Cells. *J. Am. Chem. Soc.* **2011**, *133*, 2795–2797.
22. Gensel, J.; Borke, T.; Pérez, N. P.; Fery, A.; Andreeva, D. V.; Betthausen, E.; Müller, A. H. E.; Möhwald, H.; Skorb, E. V. Cavitation Engineered 3D Sponge Networks and Their

Application in Active Surface Construction. *Adv. Mater.* **2012**, *24*, 985–989.
23. Carter, J. L.; Drachuk, I.; Harbaugh, S.; Kelley-Loughnane, N.; Stone, M.; Tsukruk, V. V. Truly Nonionic Polymer Shells for the Encapsulation of Living Cells. *Macromol. Biosci.* **2011**, *11*, 1244–1253.
24. Georgieva, R.; Moya, S.; Donath, E.; Bäumler, H. Permeability and Conductivity of Red Blood Cell Templated Polyelectrolyte Capsules Coated with Supplementary Layers. *Langmuir* **2004**, *20*, 1895–1900.
25. Wattendorf, U.; Kreft, O.; Textor, M.; Sukhorukov, G. B.; Merkle, H. P. Stable Stealth Function for Hollow Polyelectrolyte Microcapsules Through a Poly(Ethylene Glycol) Grafted Polyelectrolyte Adlayer. *Biomacromolecules* **2007**, *9*, 100–108.
26. Drachuk, I.; Shchepelina, O.; Harbaugh, S.; Kelley-Loughnane, N.; Stone, M.; Tsukruk, V. V. Cell Surface Engineering with Edible Protein Nanoshells. *Small* **2013**, *9*, 3128–3137.
27. Ye, C.; Shchepelina, O.; Calabrese, R.; Drachuk, I.; Kaplan, D. L.; Tsukruk, V. V. Robust and Responsive Silk Ionomer Microcapsules. *Biomacromolecules* **2011**, *12*, 4319–4325.
28. Ye, C.; Drachuk, I.; Calabrese, R.; Dai, H.; Kaplan, D. L.; Vladimir, V.; Tsukruk, V. V. Permeability and Micromechanical Properties of Silk Ionomer Microcapsules. *Langmuir* **2012**, *28*, 12235–12244.
29. Magennis, E. P.; Fernandez-Trillo, F.; Sui, C.; Spain, S. G.; Bradshaw, D. J.; Churchley, D.; Mantovani, G.; Winzer, K.; Alexander, C. Bacteria-Instructed Synthesis of Polymers for Self-Selective Microbial Binding and Labelling. *Nat. Mater.* **2014**, *13*, 748–755.
30. Xu, L.; Ankner, J. F.; Sukhishvili, S. A. Steric Effects in Ionic Pairing and Polyelectrolyte Interdiffusion within Multilayered Films: A Neutron Reflectometry Study. *Macromolecules* **2011**, *44*, 6518–6524.
31. Shiratori, S. S.; Rubner, M. F. pH-Dependent Thickness Behavior of Sequentially Adsorbed Layers of Weak Polyelectrolytes. *Macromolecules* **2000**, *33*, 4213–4219.
32. Sui, Z.; Salloum, D.; Schlenoff, J. B. Effect of Molecular Weight on the Construction of Polyelectrolyte Multilayers: Stripping *Versus* Sticking. *Langmuir* **2003**, *19*, 2491–2495.
33. Glinel, K.; Déjugnat, C.; Prevot, M.; Schöler, B.; Schönhoff, M.; Klitzing, R. V. Responsive Polyelectrolyte Multilayers. *Colloids Surf., A* **2007**, *303*, 3–13.
34. Hsu, B. B.; Hagerman, S. R.; Jamieson, K.; Veselinovic, J.; Neill, N. O.; Holler, E.; Ljubimova, J. Y.; Hammond, P. T. Multilayer Films Assembled from Naturally-Derived Materials for Controlled Protein Release. *Biomacromolecules* **2014**, *15*, 2049–2057.
35. Boudou, T.; Crouzier, T.; Ren, K.; Blin, G.; Picart, C. Multiple Functionalities of Polyelectrolyte Multilayer Films: New Biomedical Applications. *Adv. Mater.* **2010**, *22*, 441–467.
36. Decher, G. In *Multilayer Thin Films: Sequential Assembly of Nanocomposite Materials*, 2nd ed.; Decher, G., Schlenoff, J. B., Eds.; Wiley-VCH Verlag GmbH & Co. KGaA: Weinheim, 2012; pp 1−1088.
37. Zhang, R.; Köhler, K.; Kreft, O.; Skirtach, A.; Möhwald, H.; Sukhorukov, G. Salt-Induced Fusion of Microcapsules of Polyelectrolytes. *Soft Matter* **2010**, *6*, 4742–4747.
38. Wilson, J. T.; Cui, W.; Chaikof, E. L. Layer-by-layer Assembly of a Conformal Nanothin PEG Coating for Intraportal Islet Transplantation. *Nano Lett.* **2008**, *8*, 1940–1948.
39. Kozlovskaya, V.; Harbaugh, S.; Drachuk, I.; Shchepelina, O.; Kelley-Loughnane, N.; Stone, M.; Tsukruk, V. V. Hydrogen-Bonded LbL Shells for Living Cell Surface Engineering. *Soft Matter* **2011**, *7*, 2364–2372.
40. Mecke, A.; Majoros, I. J.; Patri, A. K.; Baker, J. R.; Banaszak Holl, M. M.; Orr, B. G. Lipid Bilayer Disruption by Polycationic Polymers: the Roles of Size and Chemical Functional Group. *Langmuir* **2005**, *21*, 10348–10354.
41. Kharlampieva, E.; Kozlovskaya, V. Cytocompatibility and Toxicity of Functional Coatings Engineered at Cell Surfaces. In *Cell Surface Engineering: Fabrication of Functional Nanoshells*; Fakhrullin, R. F., Choi, I. S., Lvov, Y., Eds.; The Royal Society of Chemistry, Thomas Graham House: Cambridge, U.K., 2014; pp 98−125.
42. Hunter, A. C. Molecular hurdles in Polyfectin Design and Mechanistic Background to Polycation Induced Cytotoxicity. *Adv. Drug Delivery Rev.* **2006**, *58*, 1523–1531.
43. Lee, M.; Kim, S. W. Polyethylene Glycol-Conjugated Copolymers for Plasmid DNA Delivery. *Pharm. Res.* **2005**, *22*, 1–10.
44. Zhang, X.; Pan, S. R.; Hu, H. M.; Wu, G. F.; Feng, M.; Zhang, W.; Luo, X. Poly (Ethylene Glycol)-Block-Polyethylenimine Copolymers as Carriers for Gene Delivery: Effects of PEG Molecular Weight and PEGylation Degree. *J. Biomed. Mater. Res., Part A* **2008**, *84*, 795–804.
45. Wilson, J. T.; Cui, W.; Kozlovskaya, V.; Kharlampieva, E.; Pan, D.; Qu, Z.; Krishnamurthy, V. R.; Mets, J.; Kumar, V.; Wen, J.; *et al.* Cell Surface Engineering with Polyelectrolyte Multilayer Thin Films. *J. Am. Chem. Soc.* **2011**, *133*, 7054–7064.
46. Wilson, J. T.; Krishnamurthy, V. R.; Cui, W.; Qu, Z.; Chaikof, E. L. Noncovalent Cell Surface Engineering with Cationic Graft Copolymers. *J. Am. Chem. Soc.* **2009**, *131*, 18228–18229.
47. Raghavendra, P.; Skirtach, A. G.; Kreft, O.; Bédard, M.; Garstka, M.; Gould, K.; Möhwald, H.; Sukhorukov, G. B.; Winterhalter, M.; Springer, S. Controlled Intracellular Release of Peptides from Microcapsules Enhances Antigen Presentation on MHC Class I Molecules. *Small* **2009**, *5*, 2168–2176.
48. Serban, M. A.; Kaplan, D. L. pH-Sensitive Ionomeric Particles Obtained *via* Chemical Conjugation of Silk with Poly-(Amino Acid)s. *Biomacromolecules* **2010**, *11*, 3406–3412.
49. Zhou, C. Z.; Confalonieri, F.; Jacquet, M.; Perasso, R.; Li, Z. G.; Janin, J. Silk Fibroin: Structural Implications of a Remarkable Amino Acid Sequence. *Proteins: Struct., Funct., Bioinf.* **2001**, *44*, 119–122.
50. Asakura, T.; Suita, K.; Kameda, T.; Afonin, S.; Ulrich, A. S. Structural Role of Tyrosine in *Bombyx mori* Silk Fibroin, Studied by Solid-State NMR and Molecular Mechanics on a Model Peptide Prepared as Silk I and II. *Magn. Reson. Chem.* **2004**, *42*, 258–266.
51. Lu, Q.; Zhu, H.; Zhang, C.; Zhang, F.; Zhang, B.; Kaplan, D. L. Silk Self-Assembly Mechanisms and Control From Thermodynamics to Kinetics. *Biomacromolecules* **2012**, *13*, 826–832.
52. Kharlampieva, E.; Sukhishvili, S. A. Hydrogen-Bonded Layer-by-Layer Polymer Films. *J. Macromol. Sci., Part C* **2006**, *46*, 377–395.
53. Kharlampieva, E.; Sukhishvili, S. A. Polyelectrolyte Multilayers of Weak Polyacid and Cationic Copolymer: Competition of Hydrogen-Bonding and Electrostatic Interactions. *Macromolecules* **2003**, *36*, 9950–9956.
54. Prescott, Harley *Klein's Microbiology*, 7th ed.; Willey, J. M., Sherwood, L. M., Woolverton, C. J., Prescott, L. M., Eds.; McGraw-Hill Higher Education: New York, 2008; Chapters 3, 4.
55. Sutcliffe, I. C. A Phylum Level Perspective on Bacterial Cell Envelope Architecture. *Trends Microbiol.* **2010**, *18*, 464–470.
56. Eisoldt, L.; Hardy, J. G.; Heim, M.; Scheibel, T. R. The Role of Salt and Shear on the Storage and Assembly of Spider Silk Proteins. *J. Struct. Biol.* **2010**, *170*, 413–419.
57. Wong Po Foo, C.; Bini, E.; Hensman, J.; Knight, D. P.; Lewis, R. V.; Kaplan, D. L. Role of pH and Charge on Silk Protein Assembly in Insects and Spiders. *Appl. Phys. A: Mater. Sci. Process.* **2006**, *82*, 223–233.
58. Yucel, T.; Cebe, P.; Kaplan, D. L. Vortex-Induced Injectable Silk Fibroin Hydrogels. *Biophys. J.* **2009**, *97*, 2044–2050.
59. Wallet, B.; Kharlampieva, E.; Campbell-Proszowska, K.; Kozlovskaya, V.; Malak, S.; Anker, J. F.; Kaplan, D. L.; Tsukruk, V. V. Silk Layering As Studied with Neutron Reflectivity. *Langmuir* **2012**, *28*, 1181–1189.
60. Jiang, C.; Wang, X.; Gunawidjaja, R.; Lin, Y.-H.; Gupta, M. K.; Kaplan, D. L.; Naik, R. R.; Tsukruk, V. V. Mechanical Properties of Robust Ultrathin Silk Fibroin Films. *Adv. Funct. Mater.* **2007**, *17*, 2229–2237.
61. Daffe, M.; Zuber, B. In *Bacterial Membranes: The Fascinating Coat. Surrounding Mycobacteria*; Remaut, H., Fronzes, R., Eds.; Caister Academic Press: Norfolk, U.K., 2014; pp 179−192.

62. Matias, V. R. F.; Beveridge, T. J. Cryo-Electron Microscopy Reveals Native Polymeric Cell Wall Structure in *Bacilus subtilis 168* and the Existence of a Periplasmic Space. *Mol. Microbiol.* **2005**, *56*, 240–251.
63. Bhavsar, A. P.; Brown, E. D. Cell Wall Assembly in *Bacillus subtilis*: How Spirals and Spaces Challenge Paradigms. *Mol. Microbiol.* **2006**, *60*, 1077–1090.
64. Raetz, C. R. H.; Whitfield, C. Lipopolysaccharide Endotoxins. *Annu. Rev. Biochem.* **2002**, *71*, 635–700.
65. Caroff, M.; Karibian, D. Structure of Bacterial Lipopolysaccharides. *Carbohydr. Res.* **2003**, *338*, 2431–2447.
66. Silhavy, T. J.; Kahne, D.; Walker, S. The Bacterial Cell Envelope. *Cold Spring Harbor Perspect. Biol.* **2010**, *2*, a000414.
67. Lvov, Y. In *Protein Architecture: Electrostatic Layer-by-Layer Assembly of Proteins and Polyions*; Lvov, Y., Mohwald, H., Eds.; Marcel Dekker, Inc.: New York, 2000; pp 1−396.
68. Feuz, L.; Leermakers, F. A. M.; Textor, M.; Borisov, O. Adsorption of Molecular Brushes with Polyelectrolyte Backbones onto Oppositely Charged Surfaces: A Self-Consistent Field Theory. *Langmuir* **2008**, *24*, 7232–7244.
69. Riss, T. L.; Moravec, R. A.; Niles, A. L.; Benink, H. A.; Worzella, T. J.; Minor, L. In *Assay Guidance Manual: Cell Viability Assays*; Sittampalam, G. S., Gal-Edd, N., Arkin, M., Auld, D., Austin, C., Bejcek, B., Glicksman, M., Inglese, J., Lemmon, V., Li, Z., *et al.*, Eds.; Eli Lilly & Company and the National Center for Advancing Translational Sciences: Bethesda, MD, 2004; pp 1−23.
70. Yoon, K.-Y.; Byeon, J. H.; Park, J.-H.; Hwang, J. Susceptibility Constants of *Escherichia coli* and *Bacillus subtilis* to Silver and Copper Nanoparticles. *Sci. Total Environ.* **2007**, *373*, 572–575.
71. Ho, C. H.; Tobis, J.; Sprich, C.; Thomann, R.; Tiller, J. C. Nanoseparated Polymeric Networks with Multiple Antimicrobial Properties. *Adv. Mater.* **2004**, *16*, 957–961.
72. Munoz-Bonilla, A.; Fernandez-Garcia, M. Polymeric Materials with Antimicrobial Activity. *Prog. Polym. Sci.* **2012**, *37*, 281–339.
73. Fischer, D.; Li, Y. X.; Ahlemeyer, B.; Krieglstein, J.; Kissel, T. *In Vitro* Cytotoxicity Testing of Polycations: Influence of Polymer Structure on Cell Viability and Hemolysis. *Biomaterials* **2003**, *24*, 1121–1131.
74. Topp, S.; Reynoso, C. M. K.; Seeliger, J. C.; Goldlust, I. S.; Desai, S. K.; Murat, D.; Shen, A.; Puri, A. W.; Komeili, A.; Bertozzi, C. R.; *et al.* Synthetic Riboswitches That Induce Gene Expression in Diverse Bacterial Species. *Appl. Environ. Microbiol.* **2010**, *76*, 7881–7884.
75. Breaker, R. R. Prospects for Riboswitch Discovery and Analysis. *Mol. Cell* **2011**, *43*, 867–879.
76. Berens, C.; Suess, B. Riboswitch Engineering—Making the All-Important Second and Third Steps. *Curr. Opin. Biotechnol.* **2015**, *31*, 10–15.
77. Waters, L. S.; Storz, G. Regulatory RNAs in Bacteria. *Cell* **2009**, *136*, 615–628.
78. Davidson, M. E.; Harbaugh, S. V.; Chushak, Y. G.; Stone, M. O.; Kelley-Loughnane, N. Development of a 2,4-Dinitrotoluene-Responsive Synthetic Riboswitch in *E. coli* Cells. *ACS Chem. Biol.* **2012**, *8*, 234–241.
79. Winker, W. C.; Breaker, R. R. Regulation of Bacterial Gene Expression by Riboswitches. *Annu. Rev. Microbiol.* **2005**, *59*, 487–517.
80. Wang, S.; Guo, Z. Bio-Inspired Encapsulation and Functionalization of Living Cells with Artificial Shells. *Colloids Surf., B* **2014**, *113*, 483–500.
81. Ivanov, V.; Chu, J. Applications of Microorganisms to Geotechnical Engineering for Bioclogging and Biocementation of Soil *in Situ*. *Rev. Environ. Sci. Bio/Technol.* **2008**, *7*, 139–153.
82. Li, Q.; Mahendra, S.; Lyon, D. Y.; Brunet, L.; Liga, M. V.; Li, D.; Alvarez, P. J. Antimicrobial Nanomaterials for Water Disinfection and Microbial Control: Potential Applications and Implications. *Water Res.* **2008**, *42*, 4591–4602.
83. Murphy, A. R.; St. John, P.; Kaplan, D. L. Modification of Silk Fibroin Using Diazonium Coupling Chemistry and the Effects on hMSC Proliferation and Differentiation. *Biomaterials* **2008**, *29*, 2829–2839.
84. Harbaugh, S.; Kelley-Loughnane, N.; Davidson, M.; Narayanan, L.; Trott, S.; Chushak, Y. G.; Stone, M. O. FRET-Based Optical Assay for Monitoring Riboswitch Activation. *Biomacromolecules* **2009**, *10*, 1055–1060.
85. Lynch, S. A.; Gallivan, J. P. A flow Cytometry-Based Screen for Synthetic Riboswitches. *Nucleic Acids Res.* **2009**, *37*, 184–192.
86. Bomati, E. K.; Haley, J. E.; Noel, J. P.; Deheyn, D. D. Spectral and Structural Comparison Between Bright and Dim Green Fluorescent Proteins in Amphioxus. *Sci. Rep.* **2014**, *4*, 1–9.
87. Pedelacq, J.-D.; Cabantous, S.; Tran, T.; Terwilleger, T. C.; Waldo, G. S. Engineering and Characterization of a Superfolder Green Fluorescent Protein. *Nat. Biotechnol.* **2006**, *24*, 79–88.
88. Hamid, R.; Rotshteyn, Y.; Rabadi, L.; Parokh, R.; Bullock, P. Comparison of Alamar Blue and MTT Assays for High Through-Put Screening. *Toxicol. In Vitro* **2004**, *18*, 703–710.
89. McConney, M. E.; Singamaneni, S.; Tsukruk, V. V. Probing Soft Matter with the Atomic Force Microscopies: Imaging and Force Spectroscopy. *Polymer Rev.* **2010**, *50*, 235–286.